Journal of Engineering Mathematics (2006) 54: 17–30
DOI 10.1007/s10665-005-7718-x
© Springer 2006

One-dimensional transient dynamic response in functionally graded layered media

I. ABU-ALSHAIKH and B. KÖKLÜCE
Department of Mathematics, Fatih University, Istanbul 34500, Turkey (E-mail: aibrahim@fatih.edu.tr)

Received 7 July 2004; accepted in revised form 9 May 2005

Abstract. In this study, one-dimensional transient wave propagation in multilayered functionally graded media is investigated. The multilayered medium consists of N different layers of functionally graded materials (FGMs), *i.e.*, it is assumed that the stiffness and the density of each layer are varying continuously in the direction perpendicular to the layering, but isotropic and homogeneous in the other two directions. The top surface of the layered medium is subjected to a uniform dynamic in-plane time-dependent normal stress; whereas, the lower surface of the layered medium is assumed free of surface tractions or fixed. Moreover, the multilayered medium is assumed to be initially at rest and its layers are assumed to be perfectly bonded to each other. The method of characteristics is employed to obtain the solutions of this initial-boundary-value problem. The numerical results are obtained and displayed in curves showing the variation of the normal stress component with time. These curves reveal clearly the scattering effects caused by the reflections and refractions of waves at the boundaries and at the interfaces of the layers. The curves also display the effects of non-homogeneity in the wave profiles. The curves further show that the numerical technique applied in this study is capable of predicting the sharp variations in the field variables in the neighborhood of the wave fronts. By suitably adjusting the material constants, solutions for the case of isotropic, homogeneous and linearly elastic multilayered media and for some special cases including two different functionally graded layers are also obtained. Furthermore, solutions for some special cases are compared with the existing solutions in the literature; very good agreement is found.

Key words: functionally graded materials, method of characteristics, plane layered media, transient dynamic response

1. Introduction

Functionally graded materials are a new generation of engineering materials which are continuously or discretely changing their thermal and mechanical properties at the macroscopic or continuum scale [1, pp. 107–113]. Functionally graded materials are increasingly expected to be used in structural applications where high strength-to-weight and stiffness-to-weight ratios are required. These applications involving severe thermal gradients, ranging from thermal structures in advanced aircraft and aerospace engines to microelectronics. Example applications, including pressure vessels and pipes in nuclear reactors, can be found in the review papers [2] and [3]. In such applications a metallic-rich region of a functionally graded material is exposed to low temperature with a gradual microstructural transition in the direction of the temperature gradient, while a ceramic-rich region is exposed to high temperature. Among a few recent books including a comprehensive treatment of the science and technology of functionally graded materials, one can mention [4, pp. 29–63] and [5, pp. 112–120].

Several models for the case where a dynamic load is applied to the outer boundaries of a functionally graded composite body have been studied in the literature. Five models, for example, are presented in [6]; two of these simulate fiber phases in which the material is modelled as layers of different volume fractions and three simulate particle phases, where the

material properties are considered to change continuously in the thickness direction. Accordingly, two models may be used to deal with transient dynamic response in the inhomogeneous bodies; they are the homogeneous layered model and the inhomogeneous continuous model. In the first type, the FGM layer is subdivided into a large number of homogeneous thin layers, each of which has its own constant volume fraction [7]. In the second kind, the FGM plate is subdivided into inhomogeneous layers whose material properties are varying continuously in the direction perpendicular to the layering [8, 9]. In these papers Ohyoshi has developed an analytical method using an approach involving linearly inhomogeneous layer elements to investigate waves through inhomogeneous structures.

Due to the fact that the material properties of functionally graded materials are functions of one or more space variables, wave-propagation problems related to functionally graded materials are generally difficult to analyze without employing some numerical approaches. Numerical solutions of one-dimensional stress-wave propagation in an FGM plate subjected to shear or normal tractions are discussed in [10–13]. In these studies, the material properties are assumed to vary in the thickness direction and the FGM plate is divided into linearly inhomogeneous elements [10] or quadratic inhomogeneous layer elements [11, 12], whereas in [13], the material properties of the FGM plate throughout the thickness direction are assumed to be functions with arbitrary powers. Two-dimensional transient-wave-propagation problems in an FGM plate have, recently, been discussed by applying a composite wave-propagation algorithm in [14, 15], and using finite elements with graded properties in [16] to simulate elastic wave propagation in continuously nonhomogeneous materials. However, to the authors' the best knowledge, the transient dynamic response of a multilayered FGM body subjected to a uniform pressure wavelet has not been investigated in the literature.

In this paper, the method of characteristics is employed to obtain the solutions. This method has been employed effectively in investigating one- and two-dimensional transient-wave-propagation problems in multilayered plane, cylindrical and spherical homogeneous layered media [17–19]. In these references, the multilayered medium consists of N layers of isotropic, homogeneous and linearly elastic or viscoelastic material with one or two relaxation times. A brief review on combining the method of characteristics with Fourier transforms to investigate two-dimensional transient wave propagation in viscoelastic homogeneous layered media can be found in [20–21]. It is well known that, for the one-dimensional homogeneous case, the characteristic manifold consists of straight lines in the zt-plane (here, t: time; z: space variable) and the canonical equations holding on them are ordinary differential equations which can be integrated accurately using a numerical method, *e.g.* an implicit trapezoidal-rule formula [17–21]. However, in functionally graded material the characteristic manifold consists of nonlinear curves in the zt-plane and the canonical equations can be integrated approximately along the characteristic curves by employing a small-time discretization. This step-by-step numerical technique is capable of describing the sharp variation of the disturbance in the neighborhood of the wave front without showing any sign of instability. Hence, as will be shown in this study, the method of characteristics can be used conveniently for one-dimensional transient wave propagation through functionally graded materials, and we believe that it can be combined with a transformation technique to handle two-dimensional transient wave propagation in multilayered functionally graded materials, as well.

2. Formulation of the problem

The multilayered medium considered in this study is of thickness H and it consists of N different FGM layers. It is referred to a Cartesian co-ordinate system (x, y, z), in which the

xy-plane coincides with the upper surface of the layered medium and the z-axis is directed downward; Figure 1. The material properties in each layer are assumed to be vary continuously in the z-direction, but isotropic and homogeneous in the other two directions. The upper surface of the layered medium is subjected to a uniform time-dependent pressure wavelet; the lower surface is assumed to be either free of surface traction or fixed, or is subjected to a surface traction similar to that applied at the upper surface; Figure 1. The FGM layers of the composite medium are assumed to be perfectly bonded to each other. Furthermore, the layered medium is assumed to be initially at rest. In the formulation, it is assumed that the surface traction is an arbitrary function of time t, but uniform and extends to infinity over the xy-plane. Thus, the problem is a one-dimensional plane-strain problem with displacement components u_x and u_y vanishing identically and the displacement component in the z-direction being a function of z and t, *i.e.*,

$$u_z = u_z(z,t), \quad u_x = u_y = 0. \tag{1}$$

Thus, the stress equation of motion, in the absence of body forces, for a typical FGM layer can be written as

$$\frac{\partial \tau_{zz}}{\partial z} = \rho \frac{\partial v_z}{\partial t}, \tag{2}$$

where τ_{zz} is the normal-stress component in the z-direction, ρ is the mass density of the typical layer considered and v_z is the component of the particle velocity in z-direction, *i.e.*,

$$v_z = \frac{\partial u_z}{\partial t}. \tag{3}$$

The non-vanishing stress component can be written as

$$\tau_{zz} = c\varepsilon_{zz}, \tag{4}$$

where ε_{zz} is the strain component which is related to the displacement component u_z through

$$\varepsilon_{zz} = \frac{\partial u_z}{\partial z}. \tag{5}$$

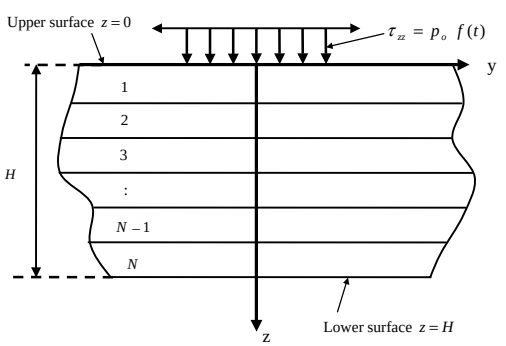

Figure 1. A plane layered medium consists of N different FGM layers subjected to uniform pressure.

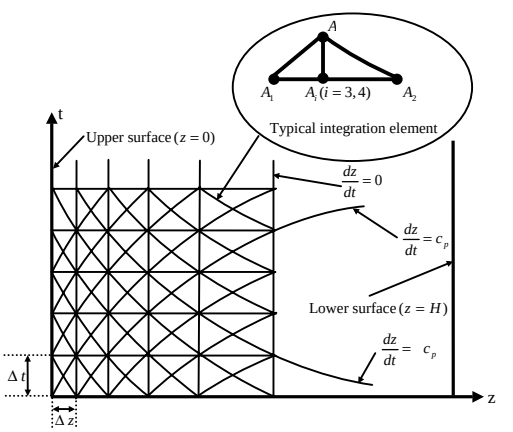

Figure 2. Network of characteristic curves on the zt-plane.

In (2) and (4) the stiffness c ($c = 2\mu + \lambda$) and the mass density ρ of the medium are assumed to be vary continuously in the z-direction, but homogeneous and isotropic in the x and y-directions, that is,

$$c = (2\mu_0 + \lambda_0)(a + bz)^m, \qquad \rho = \rho_0(a + b_\rho z)^n, \tag{6}$$

where a, b and b_ρ are dimensionless constants representing the gradients of the typical FGM layer. The parameters c_0 ($c_0 = 2\mu_0 + \lambda_0$) and ρ_0 are, respectively, the stiffness and mass density at a referred surface of the typical layer. Similar forms of (6) with $a = 1$ and $m = n = 1$ in [10], with $a = 1$ and $m = n = 2$ [11, 12] and with $a = 1$ and $b = b_\rho$ [13], were used in investigating one-dimensional transient wave propagation in an FGM plate subjected to a uniform pressure wavelet at one of its outer boundaries. Thus, this new model, given in (6), has the ability to represent all models presented in [10–13]. It will be shown later that the method applied in this study is applicable for different values of the constants appearing in Equation (6), particularly for the real constants m and n, whereas in other works it is needed to change the formulation of the problem according to how these values are changing. This general form of (6) is selected because it is suitable for a multilayered medium that consists of more than one FGM layer.

In view of Equation (6), the constitutive Equations (2–5), can be combined in one equivalent equation (wave equation), in terms of the displacement component u_z, as

$$c\frac{\partial^2 u_z}{\partial z^2} + \frac{dc}{dz}\frac{\partial u_z}{\partial z} = \rho\frac{\partial^2 u_z}{\partial t^2}. \tag{7}$$

In this paper, it is required to solve (7), satisfying the boundary, initial and interface conditions. The boundary condition at the upper surface ($z = 0$) of the multilayered medium is a time-dependent pressure pulse defined as

$$\tau_{zz}(0, t) = -p_o f(t), \tag{8}$$

where p_o is the intensity of the applied load and $f(t)$ is a prescribed function of t. The lower surface ($z = H$) is assumed to be either free of surface traction, fixed or it can be assumed to be subjected to the same loads applied at the upper surface; *viz*. Equation (8). Hence, the free or fixed boundary conditions can be written, respectively, as

$$\tau_{zz}(H, t) = 0 \quad \text{or} \quad u_z(H, t) = 0. \tag{9}$$

In the method employed in this study, we note that other alternatives for boundary conditions, such as mixed-mixed boundary conditions on both surfaces, *i.e.*, one component of displacement and the other component of the surface traction can be handled with equal ease on both surfaces. Furthermore, Equation (8) can be replaced by (9) at the upper boundary and (9) can be replaced by (8) at the lower boundary. The layers of the multilayered medium are assumed to be perfectly bonded to each other; hence, the interface conditions imply that the normal stress (τ_{zz}) and the displacement (u_z) are continuous across the interfaces of the layers. The multilayered medium is assumed to be initially at rest; hence, all the field variables are zero at $t \leq 0$. The formulation of the problem is now complete.

In view of Equation (6), the governing field equations, Equations (2–5), are to be applied to each layer and the solutions will be required to satisfy the interface conditions at the interfaces, the boundary conditions at upper and lower surfaces, Equations (8, 9), and quiescent initial conditions.

3. Solution of the problem

The solution is obtained by employing the method of characteristics. This technique involves first writing the hyperbolic differential equation, Equation (7), in view of Equations (2–6) as a system of first-order governing partial differential equations, in matrix form as

$$\mathbf{A}\mathbf{U}_{,t} + \mathbf{B}\mathbf{U}_{,z} + \mathbf{D} = \mathbf{0}, \tag{10}$$

where

$$\mathbf{A} = \mathbf{I}, \tag{11}$$

with $\mathbf{I}$ being a (4×4) identity matrix. In Equation (10), $\mathbf{B}$ is (4×4) square matrix with the elements all zero except

$$b_{14} = -c, \quad b_{24} = -1, \quad b_{42} = -\frac{c}{\rho}, \tag{12}$$

$\mathbf{D}$ is a four-dimensional column vector with nonzero elements

$$d_3 = -v_z, \quad d_4 = -\frac{\varepsilon_{zz}}{\rho}\left(\frac{\mathrm{d}c}{\mathrm{d}z}\right), \tag{13}$$

and $\mathbf{U}$ is a four-dimensional column vector containing the unknown field variables:

$$\mathbf{U} = (\tau_{zz}, \varepsilon_{zz}, u_z, v_z)^T, \tag{14}$$

where T designates the transpose. In Equation (10), a comma denotes partial differentiation:

$$\mathbf{U}_{,t} = \frac{\partial \mathbf{U}}{\partial t}, \mathbf{U}_{,z} = \frac{\partial \mathbf{U}}{\partial z}. \tag{15}$$

The second step of the solution procedure involves the determination of the solutions of Equation (10) for each layer satisfying the conditions at the boundaries, Equations (8–9), at the interfaces and the zero initial conditions. The system of governing equations, Equation (10), is hyperbolic, and the solution is constructed by converting it into a system of first-order ordinary differential equations, each of which is valid along a different family of characteristic curves. These equations, called the canonical equations, are suitable for numerical analysis because the use of the canonical form makes it possible to obtain the solution by a step-by-step integration procedure. The convergence and numerical stability of the method are well-established; see [22, pp. 62–82], [23, pp. 114–130].

The characteristic lines, along which the canonical equations are valid, are governed by the characteristic equation

$$\det(\mathbf{B} - V\mathbf{A}) = 0, \tag{16}$$

where $V = \frac{\mathrm{d}z}{\mathrm{d}t}$. Equation (16) yields the eigenvalues $V_i (i = 1 - 4)$, which are

$$V_1 = c_p, \quad V_2 = -c_p, \quad V_3 = 0, \quad V_4 = 0, \tag{17}$$

where

$$c_p = \sqrt{\frac{c}{\rho}} = \sqrt{\frac{\lambda + 2\mu}{\rho}} = \sqrt{\frac{(2\mu_0 + \lambda_0)(a + bz)^m}{\rho_0 (a + b_\rho z)^n}}, \tag{18}$$

is the dilatational (primary, pressure, irrotational or longitudinal) wave velocity. The characteristic manifold is thus composed of the families of the curves $\frac{dz}{dt} = V_i \ (i = 1-4)$. The terms $\frac{dz}{dt} = V_1 = c_p$ and $\frac{dz}{dt} = V_2 = -c_p$ describe two characteristic families of curves with slopes (c_p) and $(-c_p)$, respectively, on the zt-plane. Further, $\frac{dz}{dt} = V_i = 0$, $(i = 3-4)$ defines straight lines parallel to the t-axis; Figure 2. The canonical equations are determined from

$$\mathbf{l}_i^T \mathbf{A} \frac{d\mathbf{U}}{dt} + \mathbf{l}_i^T \mathbf{D} = \mathbf{0}, \tag{19}$$

which holds along $\frac{dz}{dt} = V_i (i = 1-4)$. In Equation (19), $\frac{d}{dt}$ denotes the total time derivative along a characteristic line and $\mathbf{l}_i$ is the left-hand eigenvector satisfying the equation

$$(\mathbf{B}^T - V_i \mathbf{A}^T)\mathbf{l}_i = \mathbf{0}. \tag{20}$$

In view of Equations (11–12) and (17–18), the linearly independent left-hand set of eigenvectors can be determined from Equation (20). When these left-hand eigenvectors, together with **A** and **D** defined in (11) and (13), are substituted in Equation (19), the canonical equations can be obtained as

$$K_{ij} \frac{dU_j}{dt} = F_{ij} U_j, \quad (i, j = 1-4), \tag{21}$$

where the nonzero elements of K_{ij} and F_{ij}, are

$$\begin{aligned} &k_{12} = -c_p, \quad k_{22} = c_p, \quad k_{14} = k_{24} = k_{31} = 1, \\ &k_{43} = 1, \quad k_{32} = -c, \quad f_{12} = f_{21} = \tfrac{1}{\rho}\tfrac{dc}{dz}, \quad f_{44} = 1. \end{aligned} \tag{22}$$

The canonical equations are then integrated along the characteristic lines as

$$\int_{A_I}^{A} K_{ij} \frac{dU_j}{dt} dt - \int_{A_I}^{A} F_{ij} U_j \, dt = 0, \tag{23}$$

where A and A_I are points on the characteristic curves defined, respectively, at current and previous time steps as shown in the typical integration element inside Figure 2. Taking into consideration that the coefficients K_{ij} and F_{ij} are functions of z only, the above integration can be performed easily by using the trapezoidal rule [24, pp. 245–250] as

$$K_{ij} U_j(A) - K_{Ij} U_j(A_I) - \left(\frac{\Delta t}{2}\right) \{F_{ij}(A) U_j(A) + F_{Ij}(A_I) U_j(A_I)\} = 0. \tag{24}$$

Alternately, this equation can be rewritten as

$$W_{ij} U_j(A) = M_{Ij} U_j(A_I), \quad (i, j = 1-4), \tag{25}$$

where

$$W_{ij} = K_{ij} - \left(\frac{\Delta t}{2}\right) F_{ij}(A), \quad M_{Ij} = K_{Ij} + \left(\frac{\Delta t}{2}\right) F_{Ij}(A_I). \tag{26}$$

The elements of K_{ij} and F_{ij} are given in Equations (22). In Equations (24–26) there is no summation performed over the capital index $I (I = 1-4)$; therefore, Equation (25) represents four equations defined by $i = 1-4$ and for each value of the index i, there is a summation over j which takes the values $j = 1-4$. Thus, when the values of U_j are known at points $A_I (I = 1-4)$, the unknown vector at point A, $\big(U_j(A), (j = 1-4)\big)$, can be determined from (25) taking into consideration that the coefficients of K_{ij} and F_{ij}, which are functions of z only, can be found easily by the step-by-step numerical procedure discussed below. In other

words, using the mesh shown inside Figure 2, one finds the field variables at a specific point along any line parallel to the z-axis in the solution region in terms of the known field variables defined on the previous line. For this purpose, we refer to the network of the characteristic curves; Figure 2. To compute the components of the unknown vector $(U_j, (j=1-4))$ presented in (25) at every intersection point between the characteristic curves on the zt-plane, we start our solution on the network from the z-axis, where the values of all field variables are zero due to zero initial conditions, and advance into the solution region by computing U_j at the intersection points of the network between the upper and the lower boundary along the lines $t=\triangle t$, $t=2\triangle t$, $t=3\triangle t$, ..., $t=J_{\max}\triangle t$ ..... etc. To explain this numerical procedure we refer to four different locations of the typical integration element. First, if the typical integration element is located at the upper boundary, then the first equation of (25), which is valid along the line AA_1 is replaced by the boundary condition applied at the upper boundary. Second, if the integration element is an interior element, then the procedure involves the determination of the values of the unknown vector at a point A in terms of its values at A_1, A_2 and A_i, $(i=3-4)$ using (25). Third, if a point A of an integration element is located at an interface between two different layers, then the first two equations are replaced by the interface continuity conditions, whereas, in this case the number of field variables becomes double at that point. Finally, the second equation of (25) is replaced by the boundary condition applied at the lower boundary, if the typical integration element lies at that boundary. This procedure is repeated as we proceed along the t-axis, for example along the line $t=2\Delta t$, instead of using the initial conditions along the line $t=0$; we use the field variables which are computed in the previous step along the line $t=\Delta t$. This process is repeated until we get results for a sufficient value of t, for example $t=J_{\max}\triangle t$, where $J_{\max}$ is the maximum number of intervals considered in the t-direction.

4. Numerical results and discussion

First, three examples will be given to verify the validity of the numerical technique employed in this study. Then, one example involving the dynamic response of an FGM layered medium consists of more than one FGM layer will be studied.

4.1. Verification problems

4.1.1. *Verification problem 1*

The first example of verification is a single isotropic, elastic and nonhomogeneous layer subjected to a uniform normal traction at $z=H$ with a rectangular pulse in time. In our formulation, the rectangular pulse is simulated by the trapezoidal distribution shown in Figure 3(b), with $e=\Delta t=0{\cdot}0122$ μs, $d=50$ μs and $p_o=-1000$ psi. The upper surface $(z=0)$ is assumed to be fixed. Numerical results are presented with the following parameters: $\rho_0=0{\cdot}0733$ lb$_f$ s^2/in^4, $m=0$, $n=-2$, $a=1$, $b=0$, $b_\rho=0{\cdot}\overline{87804}$, $c_0=120\times10^6$ psi. These properties correspond to a constant stiffness and a variable density that starts from $\rho_0=0{\cdot}0733$ lb$_f$ s^2/in^4 at the upper surface to $\rho=0{\cdot}000733$ lb$_f$ s^2/in^4 at the lower surface $(z=H=10{\cdot}25$ in). Numerical treatment of this problem by the use of finite elements with graded properties was given, recently, in [16]. The solution of this problem in our treatment is obtained as a special case of a multilayered medium consisting of four layers with thicknesses $h_{(i)}=2{\cdot}5625$, where $\overline{h}_{(i)}$ is the thickness of the i-th layer. In Figure 3(a), the variation of the normal stress τ_{zz} with time at the location near the middle surface of the plate $(z=5{\cdot}125)$, is shown. The solution of the FGM layer is compared with the finite-element solution presented in [16]; a good agreement is found between the two solutions. The curves of Figure 3(a) clearly display the effects of

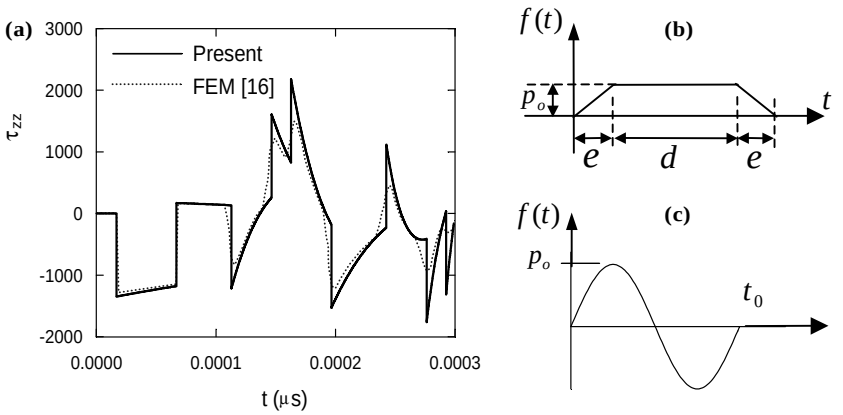

Figure 3. (a) Time variation of the normal stress (τ_{zz}) at $z = 5{\cdot}125$ for a single FGM layer. (b) and (c) Time variations of the applied load.

reflections from the lower and upper surfaces and the homogeneity effects which are indicated by (i) the significant difference between the amplitude applied at lower surface and the amplitude of the stress wave in the FGM plate and (ii) the time of the arrival of disturbances in the FGM layer is earlier than that of the corresponding homogeneous plate whose mass density is equal to the value at the upper surface. This is because the longitudinal wave velocity of the FGM plate is higher than that of the corresponding homogeneous plate. The numerical results further show that the applied numerical technique has the ability of predicting the sharp variations at the wave fronts without showing any sign of instability or noise.

4.1.2. *Verification problem 2*

In the second example of verification, a single FGM plate excited by an incident pressure wave on the bottom surface of the plate is considered. In this example, the numerical computations have been carried out and the results are displayed in terms of non-dimensional quantities. These dimensionless quantities are taken in terms of the thickness of the FGM plate (H) and the density and stiffness at the middle surface of the plate. Thus, the non-dimensional time $\bar{t} = 1$ is the time required for the wave velocity at the middle surface to travel once over the thickness of the corresponding homogeneous plate. Note here that the non-dimensional

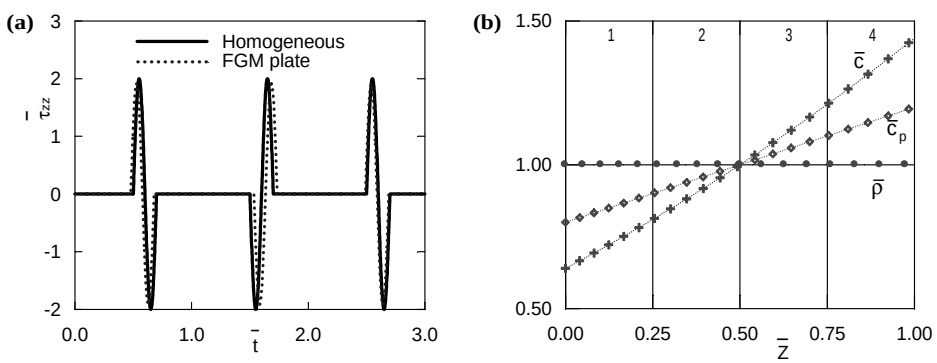

Figure 4. (a) Variation of the non-dimensional normal stress $\bar{\tau}_{zz}$ with non-dimensional time $\bar{t}$ at the midpoint ($\bar{z} = 0{\cdot}5$). (b) Space variation of non-dimensional density ($\bar{\rho}$), stiffness ($\bar{c}$) and wave velocity ($\bar{c}_p$) in terms of material properties at the midpoint of the FGM plate.

quantities are designated by bars. This problem has been solved in [10] and [12] using the linearly inhomogeneous element and quadratic-layer-element approaches, respectively.

The normal stress applied at the bottom surface of the plate ($\bar{z} = \overline{H} = 1$) is given as [10, 12]

$$\tau_{zz}(H, t) = -p_o \sin(10\pi t), \tag{27}$$

where $\overline{p}_o = 2$ is the non-dimensional intensity of the applied surface pressure with $0 \leq \bar{t} \leq 0{\cdot}2$, namely, the pressure wave applied is one cycle of a sine function with $t_0 = 2$; Figure 3(c). The upper surface of the FGM plate is assumed to be free of surface traction. The solution of this problem in our treatment is obtained as a special case of a multilayered medium consisting of four FGM layers with thicknesses $\overline{h}_{(i)} = \frac{\overline{H}}{4} = 0{\cdot}25$, where $\overline{h}_{(i)}$ is the thickness of the i-th layer. The values of b, b_ρ and a assigned for the four layers are $b = 0{\cdot}5$, $b_\rho = 0$ and $a = 1$ with $m = n = 1$ [10], *i.e.*, the mechanical properties of the linear FGM plate vary linearly in the thickness direction; Figure 4(b). To investigate how a stress wave propagates, the time history of the non-dimensional normal stress $\overline{\tau}_{zz}$ at the midpoint in the FGM plate together with that in a homogeneous plate are shown in Figure 4(a). For the homogeneous plate whose elastic constants and mass density are equal to the values at the midpoint of the FGM plate, the gradient constants are taken as $a = 1$ with $b_\rho = 0 = b$. The results obtained from the present study and those of [10] and [12], which are not shown in Figure 4(a), are almost identical. The curves of Figure 4(a) clearly display the effects of reflections from the free surfaces of the plate. Since the pressure wavelet is applied on the lower surface where the wave velocity of the FGM plate is higher than that of the homogeneous plate, the stress wave propagates faster in the lower half ($0{\cdot}5 < z < 1$). On the other hand, when the stress wave propagates in the upper half ($0 < z < 0{\cdot}5$) of the FGM plate, the wave velocity in the homogeneous plate is higher than that of the FGM plate. This can be clearly seen in Figure 4(a) where the time of the arrival of the disturbances in the FGM layer is earlier than that of the corresponding homogeneous plate; moreover, the solid line is lagging behind during the time $0 < \bar{t} < 0{\cdot}7$, and then overtaking during $0{\cdot}7 < \bar{t} < 1{\cdot}7$. As the time increases, the solid line will again be overtaken by the dashed line, and so on. Furthermore, in the curves of Figure 4(a) it is observed that the stress levels in the FGM plate are slightly less than that in the homogeneous plate. This is because the load is applied on the stiffer side of the FGM plate.

4.1.3. *Verification problem 3*

In the last example of verification, we present some results for multilayered media consist of four layers ($N = 4$), denoted as layers 1, 2, 3 and 4, with layer sequence starting from the top layer, as 1/2/3/4. In these results, we take the geometric and material properties of the four layers the same (thus, the layered system represents a single homogeneous or nonhomogeneous layer). The FGM composite consists of nickel (Ni) and zirconia (ZrO_2); on one surface the layer is pure nickel and on the other surface pure zirconia, and the material properties in-between these two surfaces vary smoothly in the thickness direction. The material properties of the constituent materials are given in Table 1. The numerical computations have been carried out and the results are displayed in terms of non-dimensional quantities. These dimensionless quantities are taken in terms of the thickness of the layered medium ($H = 5$ mm), the density and stiffness at the upper surface ($z = 0$), *i.e.*, the following non-dimensional quantities will always be true on the top surface of the first layer: $(2\overline{\mu}_0 + \overline{\lambda}_0) = \overline{\rho}_0 = \overline{c}_p = 1$. The bottom surface ($\bar{z} = \overline{H} = 1$) is subjected to a uniform normal stress defined as [13]

$$\tau_{zz}(1, t) = -p_o [H(t) - H(t - t_0)], \tag{28}$$

Table 1. Properties of materials used in examples.

Material	μ(GPa)	λ(GPa)	ρ(Kg/m^3)
Ni(Nickel)	79·0076	128·9071	8900
ZrO_2(Zirconia)	56·7669	110·1946	5331

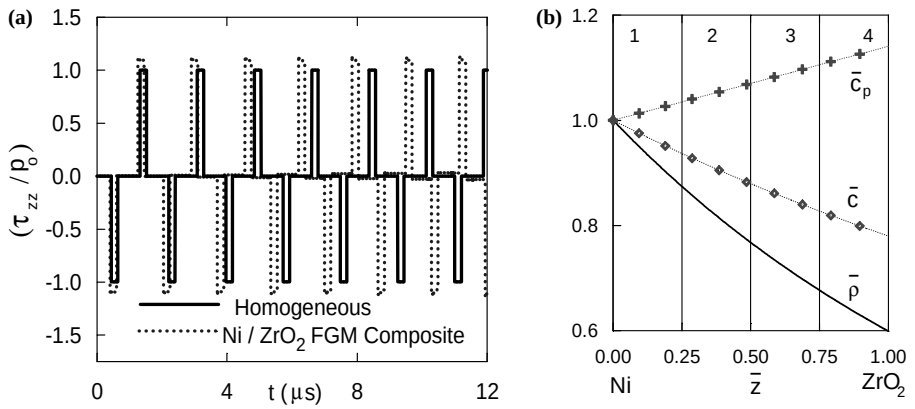

Figure 5. (a) Variation of (τ_{zz}/p_o) with t in Ni/ZrO_2 FGM composite and in homogeneous layer at $\bar{z}=0{\cdot}5$ under free/free boundary conditions. (b) Variation of non-dimensional density $(\bar{\rho})$, stiffness $(\bar{c})$ and wave velocity $(\bar{c}_p)$ with $\bar{z}$ in Ni/ZrO_2 FGM composite.

where p_o is the load intensity and $H(t)$ represents a unit step function with an initial ramp. The incident pressure wave applied at the bottom surface is equivalent to the trapezoidal distribution shown in Figure 3(b), where $t_0=d$ and $e=\triangle t$ are taken as 0·2 and 0·001 μs, respectively.

Here, we consider two problems, both are subjected to the trapezoidal pulse given by Equation (28). These problems are: nickel-zirconia (Ni/ZrO_2) FGM composite with free upper boundary condition and zirconia-nickel (ZrO_2/Ni) FGM composite with fixed upper boundary condition. In the present method, these problems are treated as special cases of the general formulation for multilayered functionally graded media by assuming that the FGM composite consists of four similar layers with $\bar{h}_{(i)}=0{\cdot}25, (i=1-4)$, where $\bar{h}_{(i)}$ is the non-dimensional thickness of the i-th layer; see Figures 5(b), and 6(b). The thicknesses and the material constants of all the four layers are assumed to be the same. Thus, in terms of the non-dimensionalization, the material properties can be computed from Table 1 for the four layers as:

for the Ni/ZrO_2 FGM composite with $m=n+2$ (see Figure 5(b)),

$$\begin{aligned} &m=-1{\cdot}8866, \quad n=-3{\cdot}8866, \quad a=1, \quad b=b_\rho=0{\cdot}14096,\\ &\bar{\rho}_0=1, \quad \bar{\mu}_0=0{\cdot}27537, \quad \bar{\lambda}_0=0{\cdot}44926, \end{aligned} \tag{29}$$

and for the ZrO_2/Ni FGM composite with $m=n+2$, (see Figure 6(b)),

$$\begin{aligned} &m=-1{\cdot}8866, \quad n=-3{\cdot}8866, \quad a=1, \quad b=b_\rho=-0{\cdot}12354,\\ &\bar{\rho}_0=1, \quad \bar{\mu}_0=0{\cdot}25370, \quad \bar{\lambda}_0=0{\cdot}49260, \end{aligned} \tag{30}$$

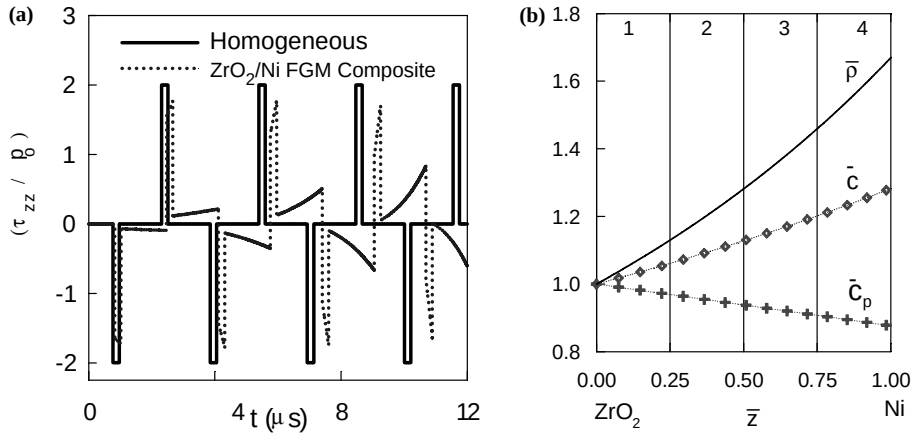

Figure 6. (a) Variation of (τ_{zz}/p_o) with t in ZrO_2/Ni FGM composite and in homogeneous layer at $\bar{z}=0$ under fixed/free boundary conditions. (b) Variation of non-dimensional density $(\bar{\rho})$, stiffness $(\bar{c})$ and wave velocity $(\bar{c}_p)$ with $\bar{z}$ in ZrO_2/Ni FGM composite.

The variation of the non-dimensional density, stiffness and dilatational wave velocity through the non-dimensional thickness for the FGM composite bodies with material properties given in Equations (29) and (30) are, respectively, shown in Figures 5(b) and 6(b). Here we should note that the propagation time of the plane wave (c_p) through the thickness of the plate $(H=5$ mm) is approximately 0·880 μs in pure nickel and 0·770 μs in pure zirconia.

In Figures 5(a) and 6(a), the variation of the dimensionless normal stress τ_{zz}/p_o with time t for the Ni/ZrO_2 FGM composite at $\bar{z}=0{\cdot}5$ and for the ZrO_2/Ni FGM composite at the upper surface $\bar{z}=0$ are shown. In Figures 5(a) and 6(a), the solutions represented by the solid line correspond to those in a homogeneous layer with $a=1$ and $b_\rho=b=0$, *i.e.*, the layers of the multilayered medium are assumed to be made of pure nickel in Figure 5(a) and of pure zirconia in Figure 6(a). Since the material constants of all the four layers are taken equal, the curves in Figures 5(a), 6(a) represent solutions for a single layer.

This one-dimensional transient-wave-propagation problem has been solved, for a single layer, in [13], using Laplace and Fourier transform techniques. There is a perfect agreement between the two solutions; for an FGM plate we have found that the absolute relative percentage error between our solutions and the analytical solutions (with $m=n+2$) presented in [13] does not exceed 0·3%. We further note that the homogeneous solutions in Figures 5(a) and 6(a) agree exactly with the known elasticity solution, as well as with the results presented in [13].

The curves of Figures 5(a) and 6(a) clearly show the effects of reflections at the top and lower surfaces through the sudden changes in the stress levels. We note further that reflections and refractions from the interfaces have disappeared; this is due to the fact that the material properties at the interfaces are constant in the homogeneous layers; however, they are varying smoothly in the thickness direction in the functionally graded composites. Moreover, we note that the stress levels in the homogeneous layer are less than those corresponding to the Ni/ZrO_2 FGM composite, Figure 5(a), and larger than those corresponding to the ZrO_2/Ni functionally graded composite; Figure 6(a). These deviations from the homogeneous material are due to the fact that the lower boundary $(\bar{z}=1)$, where the load is applied, is the stiffer side in the ZrO_2/Ni functionally graded composite, Figure 6(b), whereas, if $\bar{z}=1$ is the less stiff side, the stress levels will be higher than the corresponding stresses in the homogeneous layer; see Figure 5(b). We further observe that the time of arrival of the disturbances in the

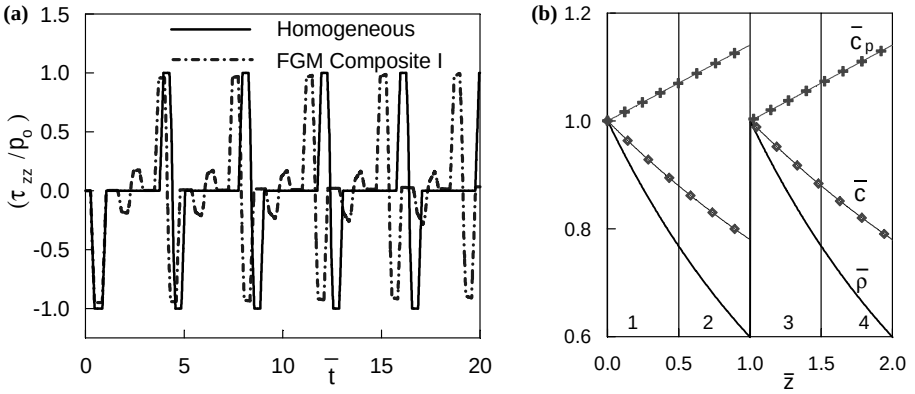

Figure 7. (a) Variation of (τ_{zz}/p_o) with non-dimensional time at $\bar{z}=0{\cdot}25$ for composite medium I under free/free boundary conditions. (b) Variation of non-dimensional density $(\bar{\rho})$, stiffness $(\bar{c})$ and wave velocity $(\bar{c}_p)$ with $\bar{z}$ in composite medium I.

Ni/ZrO_2 composite is earlier, because the wave velocity of the homogeneous layer ($\bar{c}_p=1$) is less than that of the Ni/ZrO_2 functionally graded composite; Figure 5(a). However, this situation is reversed in the ZrO_2/Ni composite, because the stress wave in the homogeneous layer is traveling faster than that in the ZrO_2/Ni functionally graded composite (see Figure 6(a)); this becomes more pronounced as time increases. We further note that, when the upper boundary is free of surface traction, the applied compressive waves are reflected as tensile waves from that boundary, Figure 5(a), and they are reflected as compressive waves when the upper boundary is fixed; Figure 6(a).

4.2. Examples for multilayered functionally graded composites

The last three verification problems provide further confidence in the validity of the numerical technique employed in this study. In this example, we consider a composite consisting of four FGM layers ($N=4$), denoted as layers 1, 2, 3 and 4, with layer sequence starting from the top layer, as 1/2/3/4. Two different multilayered media, named as I and II, are considered. For composite media I and II the four layers have the same material properties that are given by Equations (29) and (30), respectively, but a for layers 3 and 4 is taken as $a=1-b=(1-0{\cdot}14096)=0{\cdot}85904$ for composite medium I and as $a=1-b=(1-(-0{\cdot}12354))=1{\cdot}12354$ for composite medium II, where for both cases $b_\rho=b$. All the layers have the same thicknesses, *i.e.*, $\bar{h}_{(i)}=H/4=1/2$. The upper surfaces ($z=0$) of the plane laminates are subjected in time to the trapezoidal distribution shown in Figure 3(b), with $e=0{\cdot}2T$ and $d=0{\cdot}4T$, where T is a characteristic time defined by $T=H/2c_p^{(1)}$ in which H ($\overline{H}=2$) is the characteristic length and $c_p^{(1)}$ refers to the dilatational wave velocity on the top surface of the first layer. The variation of the non-dimensional density, stiffness and dilatational wave velocity through the non-dimensional thickness for composites I and II are shown in Figures 7(b) and 8(b), respectively. The curves of Figures 7(a) and 8(a), denoting the time variation of τ_{zz}/p_o at $\bar{z}=0{\cdot}25$, clearly display the effects of reflections and refractions from the interface between layers 2 and 3. We note that the applied compressive waves are reflected from the interface as compressive waves in FGM laminate I and they are reflected as tensile waves in the FGM laminate II. This is due to the fact that the bottom surface of layer 2 is stiffer than the top surface of layer 3 in composite material II, and this situation is reversed in composite material I. As time increases, we further note that the stress amplitudes of the waves reflected or refracted from

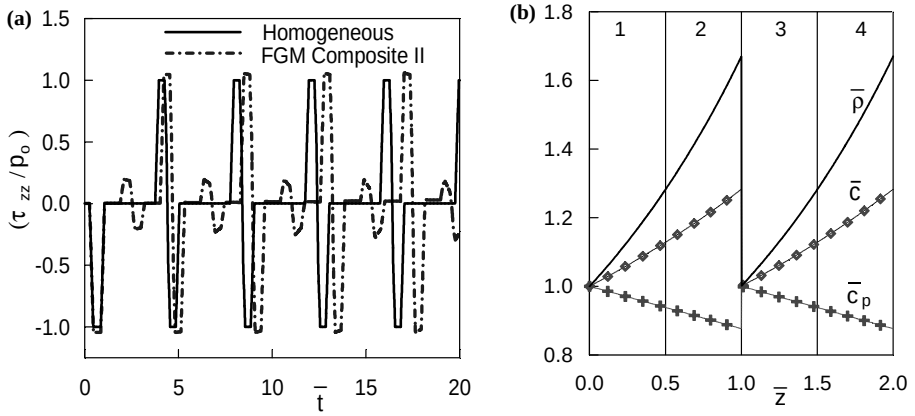

Figure 8. (a) Variation of (τ_{zz}/p_o) with non-dimensional time at $\bar{z}=0{\cdot}25$ for composite medium II under free/free boundary conditions. (b) Variation of non-dimensional density $(\bar{\rho})$, stiffness $(\bar{c})$ and wave velocity $(\bar{c}_p)$ with $\bar{z}$ in composite medium II.

the interfaces are becoming larger and larger; Figures 7(a) and 8(a). Similar trends observed in Figures 5(a) and 6(a) due to reflections and refractions at the outer boundaries and due to homogeneity effect are displayed in the curves of Figures 7(a) and 8(a) as well.

In a similar manner, we can easily treat problems involving more than two different FGM layers. For example, we can consider a composite medium consisting of eight different layers ($N=8$), with a layer sequence starting from the top surface as, 1/2/3/4/5/6/7/8, whereas the first two layers have the material properties given in Equation (29). In this case, the gradient constant a can be taken as $a=1-\kappa b$, where $b_\rho=b=0{\cdot}14096$ and $\kappa=0$ for the first pair of layers (layers 1 and 2), $\kappa=1$ for the second pair of layers (layers 3 and 4) and $\kappa=2$ and 3 for the last two pairs, respectively. Thus, the gradient constant a of a multilayered medium consist of similar-repeated FGM layers can be found by the easy sequence discussed above. This shows that the form selected in Equation (6) is suitable for a multilayered medium that consists of more than one repeated FGM layer.

5. Conclusion

One-dimensional transient stress-wave propagation in multilayered functionally graded media consisting of N different layers has been investigated. The material properties are assumed to be varying smoothly in the thickness direction. By suitable adjusting the material properties, curves for homogeneous and linearly elastic multilayered media have also been obtained. The method of characteristics is employed to obtain the solutions of the considered initial-boundary-value problem. The results show that the applied numerical technique is capable of predicting the sharp variations at the wave fronts without showing any sign of instability or noise. Furthermore, this technique properly accounts for the effects caused by reflections and refractions of waves at the boundaries and interfaces between the layers and the homogeneity effects in the wave profiles.

Based on the results obtained for an FGM layer, one may conclude that, depending on the material property grading, the location of the receiver point, boundary conditions and the amplitude of the input pulse, the resultant stress amplitudes may be greater or less than those applied at the boundary. It has been found that these amplitudes become less than those applied at the upper surface, when the upper surface ($z=0$) is stiffer than the lower surface ($z=H$) and become greater when the lower surface of an FGM layer is stiffer than the upper surface.

The method of characteristics can be combined with Fourier or Laplace transforms and used effectively in investigating two-dimensional transient dynamic response in multilayered functionally graded media. Furthermore, it can be applied effectively in investigating wave propagation through functionally graded materials exhibiting creep and relaxation under elevated temperature conditions. This is known as a viscoelastic functionally graded material whose mass density and stiffness are functions of a space variable and time. Our research in these directions is in progress.

References

1. M. Yamanouchi, M. Koizumi, M. Hirai and I. Shiota (eds.), *Proceedings of the First International Symposium on Functionally Graded Materials*. Sendai, Japan (1990).
2. Y. Tanigawa, Some basic thermoelastic problems for non-homogeneous structural materials. *Applied Mech. Rev*. 48 (1995) 287–300.
3. N. Noda, Thermal stresses in functionally graded material. *J. Thermal Stresses* 22 (1999) 477–512.
4. Y. Miyamoto, W.A. Kaysser, B.H. Rabin, A. Kawasaki and R.G. Ford, *Functionally Graded Materials: Design, Processing and Applications*. Dordrecht: Kluwer Academic Publishers (1999) 352pp.
5. S. Suresh and A. Mortensen, *Fundamentals of Functionally Graded Materials*. London: Institute of Materials, IOM Communications Ltd (1998) 165pp.
6. L. Banks-Sills, R. Eliasi and Y. Berlin, Modeling of functionally graded materials in dynamic analyses. *Composites Part B: Engineering* 33 (2002) 7–15.
7. G.R. Liu and J. Tani, Surface waves in functionally gradient piezoelectric plates. *J. Vibr. Acoust*. 116 (1994) 440–448.
8. T. Ohyoshi, Linearly inhomogeneous layer elements for reflectance evaluation of inhomogeneous layers. *Dyn. Response Behav. Compos*. 46 (1995) 121–126.
9. T. Ohyoshi, New stacking layer elements for analyses of reflection and transmission of elastic waves to inhomogeneous layers. *Mech. Res. Comm*. 20 (1993) 353–359.
10. X. Han and G.R. Liu, Effects of SH waves in functionally graded plate. *Mech. Res. Comm*. 29 (2002) 327–338.
11. G.R. Liu, X. Han and K.Y. Lam, Stress waves in functionally gradient materials and its use for material characterization. *Compos. B: Eng*. 30 (1999) 383–394.
12. X. Han, G.R. Liu and K.Y. Lam, A quadratic layer element for analyzing stress waves in functionally gradient materials and its application in material characterization. *J. Sound Vibr*. 236 (2000) 307–321.
13. T. C. Chiu and F. Erdogan, One-dimensional wave propagation in a functionally graded elastic medium. *J. Sound Vibr*. 222 (1999) 453–487.
14. A. Berezovski, J. Engelbrecht and G.A. Maugin, Numerical simulation of two dimensional wave propagation in functionally graded materials. *Eur. J. Mech*. 22 (2003) 257–265.
15. A. Berezovski, J. Engelbrecht and G.A. Maugin. Stress wave propagation in functionally graded materials. Paris:WCU 2003 (2003) 507–509.
16. M.H. Santare, P. Thamburaj and G.A. Gazoans, The use of graded finite elements in the study of elastic wave propagation in continuously non-homogeneous materials. *Int. J. Solids Structs*. 40 (2003) 5621–5634.
17. D. Turhan, Z. Celep and I.K. Zain-eddin, Transient wave propagation in layered media. *J. Sound Vibr*. 144 (1991) 247–261.
18. Y. Mengi and A.K. Tanrikulu, A numerical technique for two-dimensional transient wave propagation analyses. *Comm. Appl. Num. Meth*. 6 (1990) 623–632.
19. J.L. Wegner, Propagation of waves from a spherical cavity in an unbounded linear viscoelastic solid. *Int. J. Engng. Sci*. 31 (1993) 493–508.
20. I. Abu-Alshaikh, D. Turhan and Y. Mengi, Two-dimensional transient wave propagation in viscoelastic layered media. *J. Sound Vibr*. 244 (2001) 837–858.
21. I. Abu-Alshaikh, D. Turhan and Y. Mengi, Transient waves in viscoelastic cylindrical layered media, *Eur. J. Mech. A/Solids* 21 (2002) 811–830.
22. R. Courant and D. Hilbert, *Methods of Mathematical Physics Vol. II.* New York: Wiley-Interscience (1966) 560pp.
23. G.B Whitham, *Linear and Nonlinear Waves*. New York: Wiley (1974) 636pp.
24. C.F. Gerald and P.O. Wheately, *Applied Numerical Analysis*. USA (1984) 579pp.